Neurobiology of Disease 129 (2019) 208–216

Contents lists available at ScienceDirect

Neurobiology of Disease

journal homepage: www.elsevier.com/locate/ynbdi

Original research article

Selective vulnerability of hippocampal interneurons to graded traumatic brain injury

Jan C. Frankowski, Young J. Kim, Robert F. Hunt*

Department of Anatomy & Neurobiology, University of California, Irvine, CA 92697, USA

ARTICLE INFO

Keywords:
GABA
Interneuron
Hippocampus
Traumatic brain injury
Posttraumatic epilepsy

ABSTRACT

Traumatic brain injury is a major risk factor for many long-term mental health problems. Although underlying mechanisms likely involve compromised inhibition, little is known about how individual subpopulations of interneurons are affected by neurotrauma. Here we report long-term loss of hippocampal interneurons following controlled cortical impact (CCI) injury in young-adult mice, a model of focal cortical contusion injury in humans. Brain injured mice displayed subfield and cell-type specific decreases in interneurons 30 days after impact depths of 0.5 mm and 1.0 mm, and increasing the depth of impact led to greater cell loss. In general, we found a preferential reduction of interneuron cohorts located in principal cell and polymorph layers, while cell types positioned in the molecular layer appeared well preserved. Our results suggest a dramatic shift of interneuron diversity following contusion injury that may contribute to the pathophysiology of traumatic brain injury.

1. Introduction

Traumatic brain injury (TBI) is a serious neurological disorder that occurs after an external mechanical force damages the brain (e.g., from a bump, blow, or jolt to the head) and afflicts nearly 6 million Americans (Centers for Disease Control and Prevention, 2015). Trauma greatly increases the risk for a number of physical, cognitive, emotional, social and psychiatric health problems, and it is one of the most common causes of medically intractable epilepsy in humans (Rao and Lyketsos, 2000; Herman, 2002; Frey, 2003; Faul et al., 2010; Centers for Disease Control and Prevention, 2015; Scholten et al., 2015). Following TBI, damaged neural circuits undergo major reorganization that includes progressive neuron loss, synaptic circuit remodeling and changes in the cellular environment (Hunt et al., 2013).

As the primary source of inhibition in the brain, GABAergic interneurons coordinate information processing within cortical circuits by precisely timing and synchronizing excitatory principal populations. Such spatiotemporal control over input-output activity is achieved by a remarkable diversity of interneurons, each with distinct molecular, anatomical and electrophysiological properties (Freund and Buzsáki, 1996; Pelkey et al., 2017). In hippocampus, deficits in interneuron number or function have been implicated in a wide range of neurodegenerative disorders, such as epilepsy (de Lanerolle et al., 1989) Alzheimer's disease (Satoh et al., 1991) and stroke (Liepert et al., 2000). Studies examining brain tissue samples from patients with TBI have also found reductions in the number of interneurons in hippocampus (Swartz et al., 2006) and neocortex (Buriticá et al., 2009). These clinical findings are supported by a growing body of experimental data using in vivo rodent TBI models that display reductions in GABAergic neurons (Lowenstein et al., 1992; Toth et al., 1997; Santhakumar et al., 2000; Gupta et al., 2012; Cantu et al., 2015; Huusko et al., 2015; Butler et al., 2016; Nichols et al., 2018) and/or a marked loss of inhibition within injured regions of the brain (Li and Prince, 2002; Hunt et al., 2010; Pavlov et al., 2011; Almeida-Suhett et al., 2014, 2015; Butler et al., 2016; Nichols et al., 2018). However, it is unclear whether certain interneuron cohorts are preferentially lost after TBI as most studies focus on only a single cell type, and the effect of graded contusive injury has not been systematically evaluated.

Identifying how molecularly-distinct classes of interneurons are altered by mechanical injury is critical to understanding cortical network dysfunction in TBI and for designing precision therapies. Here, we took advantage of a widely used model of focal cortical contusion injury to directly compare and contrast the long-term effect of graded mechanical trauma on hippocampal interneuron subpopulations. We found a dramatic change in the diversity of hippocampal interneurons after contusive injury.

* Corresponding author.
E-mail address: robert.hunt@uci.edu (R.F. Hunt).

https://doi.org/10.1016/j.nbd.2018.07.022
Received 15 May 2018; Received in revised form 26 June 2018; Accepted 18 July 2018
Available online 19 July 2018
0969-9961/

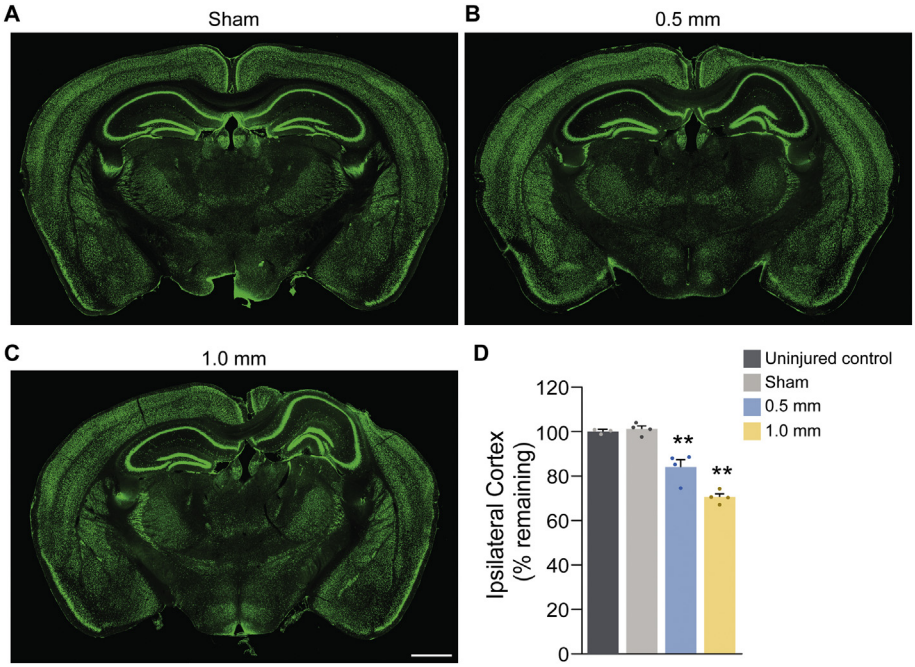

Fig. 1. Tissue damage following graded cortical contusion injury. A–C, Immunostaining for NeuN (green) in coronal sections taken from the injury epicenter in a sham-injured animal (**A**) and 30d following impact depths of 0.5 mm (**B**) or 1.0 mm (**C**). **D.** Quantification of percent cortex remaining ipsilateral to the injury. Scale bar, 1000 μm; error bars, s.e.m.; $^{**}p < .01$.

2. Methods

2.1. Animals

All experiments were first approved by the University of California, Irvine Animal Care and Use Committee and adhered to National Institutes of Health guidelines and regulations for the Care and Use of Laboratory Animals. Wild-type CD1 mice (Charles River, cat no. 022) were crossed with a hemizygous glutamic acid decarboxylase - enhanced green fluorescence protein (GAD67-GFP) knock-in line (Tamamaki et al., 2003). All animals were bred in house under a normal 12 h/12 h light/dark cycle and maintained on a CD1 background strain for > 10 generations before their use in experiments. Water and food were available ad libitum. At P60, male littermates were randomly assigned for brain injury, sham injury or no injury and experiments were performed 30d later.

2.2. Controlled cortical impact (CCI) injury

Male mice (P60) were subjected to a unilateral cortical contusion injury by controlled cortical impact (CCI) as previously described (Hunt et al., 2009, 2010, 2011, 2012; Frankowski and Hunt, 2018). Briefly, mice were anesthetized by 2% isoflurane inhalation and placed in a stereotaxic frame. The skull was exposed by midline incision, and a 4–5 mm craniotomy was made lateral to the sagittal suture and centered between bregma and lambda. The skull cap was removed, leaving the exposed underlying dura intact. The contusion device consisted of a computer-controlled, pneumatically driven impactor fitted with a beveled stainless-steel tip 3 mm in diameter (Precision Systems and Instrumentation). Brain injury was delivered using this device to compress the cortex to a depth of 0.5 mm or 1.0 mm at a velocity of 3.5 m/s and 500 ms duration. The incision was sutured, and the animal was allowed to recover for 30d. A qualitative postoperative health assessment was performed daily for 5d after TBI and periodically thereafter. All animals that received surgery were treated with buprenorphine hydrochloride (Buprenex; 0.05 mg/kg, delivered i.p.) at the time of surgery and then once daily for 3 d. We used a total of 33 mice subjected to CCI (13 at 0.5 mm depth and 20 at 1.0 mm depth), 11 mice subjected to craniotomy only (sham controls) and 7 uninjured controls. A percentage of identically treated mice have previously been shown to exhibit spontaneous seizures (Hunt et al., 2009, 2010), but mice in the present study were not monitored for seizure activity. All brain-injured mice survived and remained otherwise healthy until the day of experimentation.

2.3. Immunostaining

At P90 (30 days after CCI injury), animals were perfused transcardially with 4% paraformaldeyde (PFA) in 0.1 M PBS, pH 7.4. Brains were removed and post-fixed overnight in the same solution. Free-floating vibratome sections (50 μm) were processed using standard immunostaining procedures according to our published protocols (Hunt et al., 2013; Dinday et al., 2017). Primary antibody dilutions were as follows: chicken anti-green fluorescent protein (GFP; 1:1000; Aves, Cat No. GFP1020); mouse anti-neuronal nuclei (NeuN; 1:1000; Millipore, Cat No. MAB377), mouse anti-parvalbumin (PV; 1:500; Sigma, Cat No. P3088); rabbit anti-somatostatin (SST; 1:200; Santa Cruz, Cat No. SC-7819); rabbit anti-calretinin (CR; 1:1000; Millipore, Cat No. AB5054); rabbit anti-neuronal nitric oxide synthase (nNOS; 1:1000; Millipore, Cat No. AB5380); mouse anti-reelin (1:500; Millipore, Cat No. MAB5364). Secondary antibodies included Alexa Fluor 488 and 594 (1:1000; Life Technologies). Sections were then mounted on charged slides (Superfrost plus; Thermo Fisher Scientific) with Aqua-Mount medium.

2.4. Volumetric analysis

Volumetric analysis was performed 30 days after CCI to estimate the volume of the remaining neocortical tissue as previously described (Hall et al., 2005a). Sections were imaged using a Leica DM6 widefield fluorescence microscope with an x5 objective equipped with a motorized stage. Cortex volume was quantified by tracing the borders of the neocortex in a series of 8 NeuN-stained coronal sections containing the lesion (50 μm thick, 300 μm apart) using Imaris 9.1 software. Neocortex was defined as the region between the dorsal aspect of the corpus callosum and the pial surface. Regions of the cortical subplate (e.g., amygdala, endopiriform nucleus) were excluded from analysis. The % of the ipsilateral cortex remaining for each animal was calculated using the following formula:

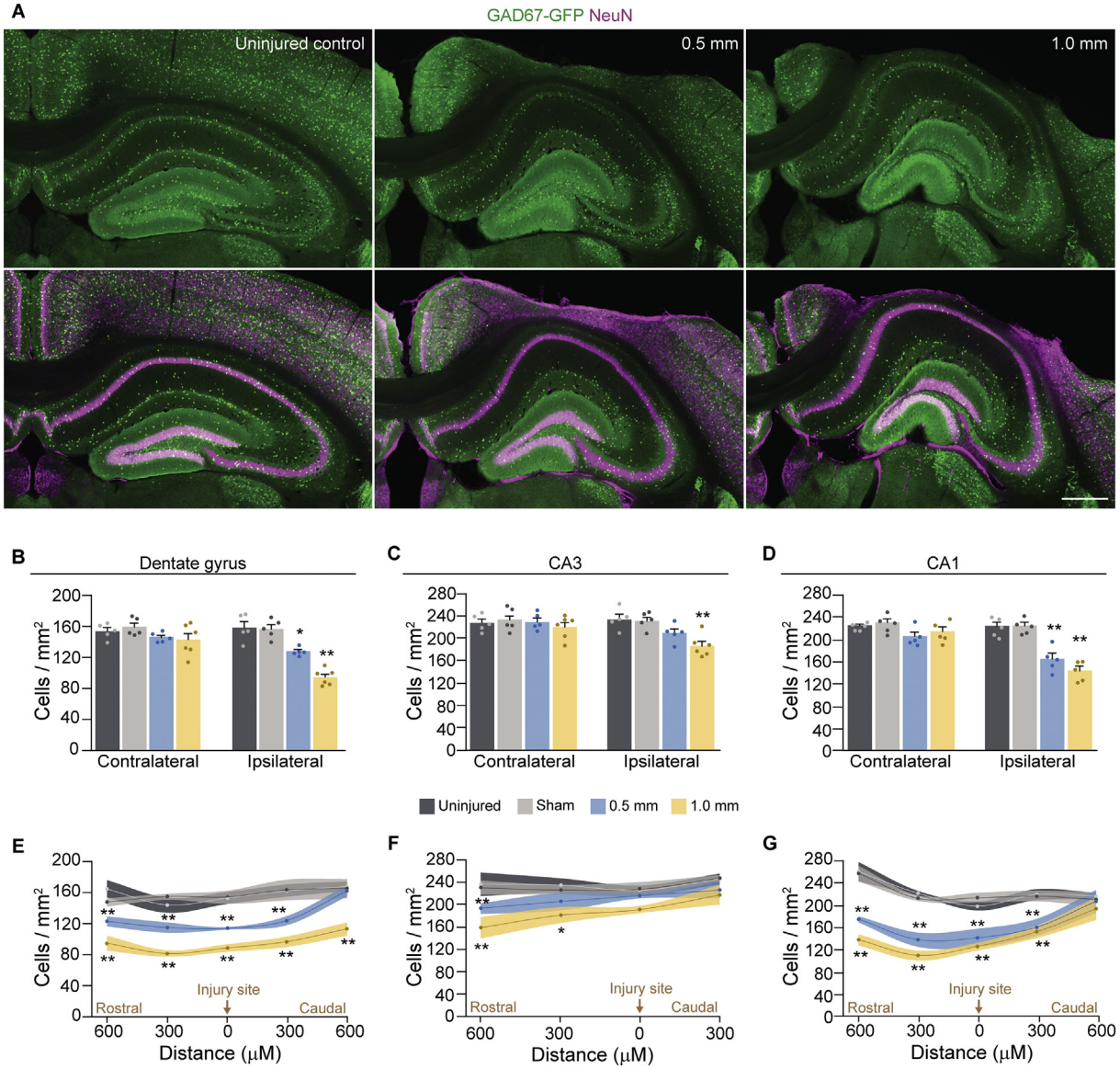

Fig. 2. Long-term reduction in interneuron density following CCI injury. A. Immunostaining for GAD67-GFP (green) and NeuN (magenta) in coronal sections taken from the injury epicenter of an uninjured animal and 30d following impact depths of 0.5 mm or 1.0 mm. **B–D.** Quantification of GAD67-GFP cell density contralateral and ipsilateral to the injury in dentate gyrus (**B**), CA3 (**C**) and CA1 (**D**). **E–G.** Quantification of GAD67-GFP cell density with distance from the injury site (zero on the *x*-axis) in ipsilateral hemisphere of dentate gyrus (**E**), CA3 (**F**) and CA1 (**G**). Scale bar, 500 μm; error bars, s.e.m.; $^{*}p < .05$, $^{**}p < .01$.

$$\% \text{ Cortex Remaining} = \left(\frac{\sum i_n}{\sum c_n} \right) \times 100$$

where i = the area of the ipsilateral cortex and c = the area of the contralateral cortex and n = the section number.

2.5. Cell quantification

Fluorescently labeled sections (50 μm) were imaged using a Leica DM6 widefield fluorescence microscope with an ×10 objective and cell counts were performed using Imaris 9.1 or ImageJ software, as described previously (Hunt et al., 2013; Dinday et al., 2017). All cells that expressed GFP (or subtype marker) were counted in every sixth coronal section in all layers of the hippocampus (300 μm apart). To define the border of hilus/CA3, straight lines were drawn from the ends of the granule cell to the proximal end of the CA3 pyramidal cell layer. For quantification of GFP+ cells in each hippocampal sub-region, four (CA3 analysis) to five (dentate gyrus and CA1 analysis) sections of the dorsal hippocampus surrounding the injury epicenter were analyzed per hemisphere for each animal and the values averaged to obtain a mean cell density (cells/mm^2). To quantify laminar distribution of GFP + cells and interneuron subtypes, three sections surrounding the injury epicenter were analyzed per hemisphere for each animal.

2.6. Statistics

Data analysis was performed using Imaris 9.1, Microsoft Excel, Graphpad Prism 6 or Systat 14 programs. Experimental groups were compared by one-way ANOVA, two-way repeated measures ANOVA followed by a Tukey's post hoc test for multiple comparisons or Chi-Square analysis. Cell layer distributions were compared by Chi-Square analysis, using the cell density for each layer (cells/mm^2). Corresponding pie charts expressed cell densities for each layer as a proportion of the sum of all layers. Data are expressed as mean ± SEM, and significance was set at $P < .05$.

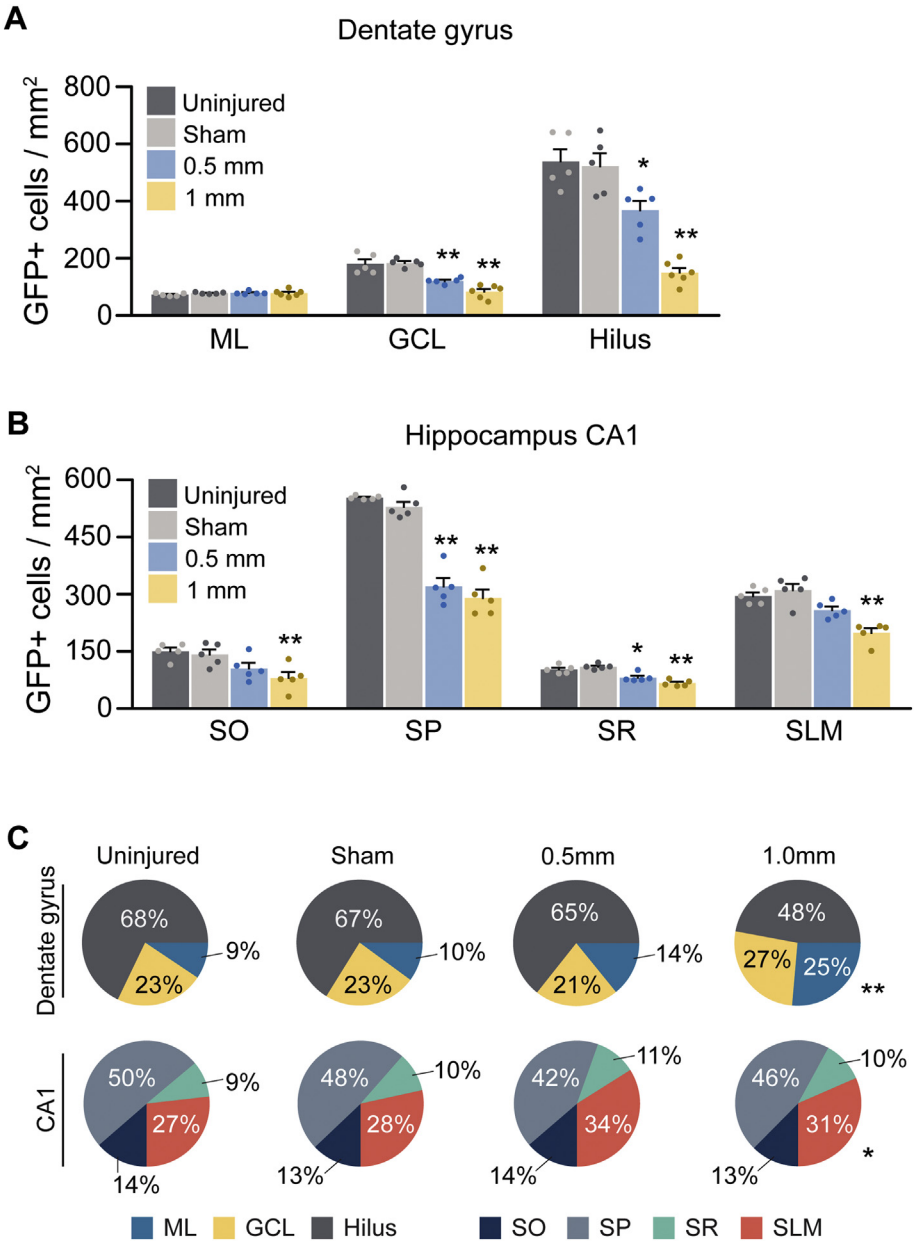

Fig. 3. Laminar distribution of hippocampal interneurons following graded CCI injury. A. Quantification of GAD67-GFP cell density in dentate gyrus ipsilateral to CCI injury. **B.** Quantification of GAD67-GFP cell density in CA1 ipsilateral to CCI injury. **C.** Relative proportion of interneurons found in each cell layer of the dentate gyrus (top) and CA1 (bottom). ML, molecular layer; GCL, granule cell layer; SO, stratum oriens; SP, stratum pyramidale; SR, stratum radiatum; SLM, stratum lacunosum-moleculare. Error bars, s.e.m.; $*p < .05$, $**p < .01$.

3. Results

3.1. Histological responses to graded CCI injury

We first examined gross damage to the brain 30 days following either 0.5 mm or 1.0 mm depth of impact at P60. Uninjured controls and sham-injured animals showed no overt cortical lesion in any animal examined (Fig. 1A). In all mice injured at 0.5 mm impact depth, the lesion consisted of a cortical cavity restricted to neocortex ($n = 4$ animals, Fig. 1B). In mice injured at 1.0 mm depth, the injury extended through the thickness of the neocortex and included substantial distortion of the principal cell layers in hippocampus. At the impact site, loss of NeuN staining in hippocampus was evident as a thinning of the pyramidal cell layer in CA1 as well as the granule cell layer in dentate gyrus ($n = 4$ animals, Fig. 1C). Quantification of the % of ipsilateral cortex remaining at 30 days post-injury, a commonly used measure of cortical damage, revealed a significantly greater lesion in both the 0.5 mm and 1.0 mm impact groups compared to uninjured or sham-injured animals, and significantly greater cortical damage after 1.0 mm injury as compared to 0.5 mm impact depth (uninjured control: 100 ± 1%; sham: 101 ± 1%, 0.5 mm: 84 ± 3%, 1.0 mm: 71 ± 1%, $F_{(3,11)} = 49.5$, $P = 1.1E-06$, one-way ANOVA; Fig. 1D). This pattern of hippocampal cell loss and cortical damage is consistent with prior studies demonstrating graded morphological and histological injury responses following 0.5 mm or 1.0 mm impact depths (Saatman et al., 2006; Hunt et al., 2009; Pleasant et al., 2011).

3.2. Regionally localized interneuron loss in hippocampus after CCI

To visualize the long-term effect of contusion injury on hippocampal interneurons, we used a GAD67-GFP knock-in reporter line labeling nearly all GABAergic interneurons (Tamamaki et al., 2003). We first

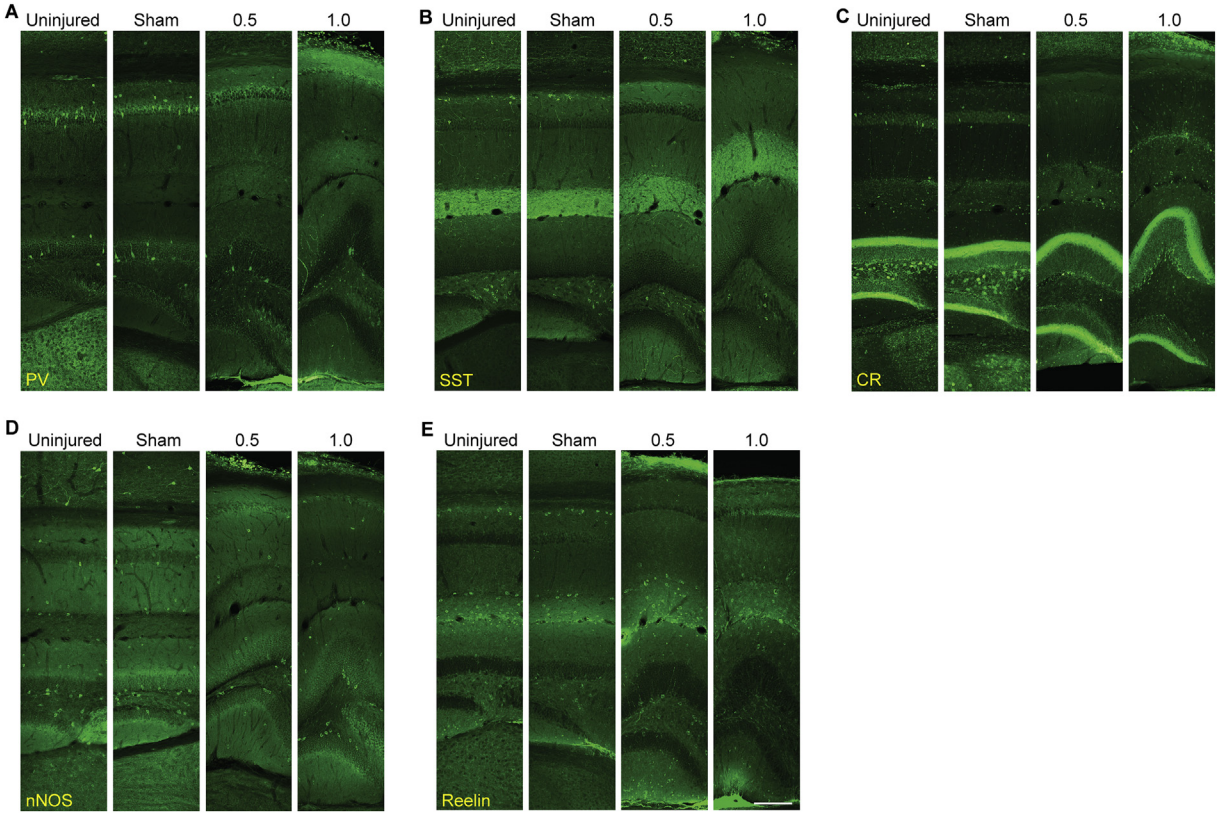

Fig. 4. Neurochemical markers of hippocampal interneurons in control and brain injured animals. A–E. Immunostaining for PV, SST, CR, nNOS and Reelin in coronal sections of hippocampus at the injury epicenter. Scale bar, 200 µm.

quantified the density of GFP+ neurons in dentate gyrus, CA3 and CA1 sub-regions of the hippocampus 30d following CCI (Fig. 2, **Table S1**). Comparisons were made between age-matched uninjured controls, animals that received only a craniotomy (sham injury) and brain injured animals that received either 0.5 mm or 1.0 mm impact. Both injury severities produced a significant reduction in GFP+ cell densities ipsilateral to the injury. In dentate gyrus, the density of GFP+ neurons was reduced by ~20% following 0.5 mm impact and ~40% following 1.0 mm impact ($F_{(7,34)}$ = 16.97, P = 2.04E-09, n = 5–6 mice per group, one-way ANOVA; Fig. 2B, **Table S1**). Cell loss was more robust after 1.0 mm injury as compared to 0.5 mm impact depth (q = 6.03, P = .003, Tukey's post hoc test), suggesting there is a correlation between increasing contusion severity and interneuron loss. In CA3, GABA neuron density was reduced only following 1.0 mm injuries (~21% reduction, $F_{(7,34)}$ = 4.77, P = 8.11E-04, n = 5–6 mice per group, one-way ANOVA; Fig. 2C). Finally, in CA1, the density of GFP+ neurons was reduced by ~26% following 0.5 mm impact and ~36% following 1.0 mm impact ($F_{(7,34)}$ = 18.02, P = 1.86E-09, n = 5 mice per group, one-way ANOVA; Fig. 2D). We did not observe a difference between the two injury severities (q = 2.82, P = .5, Tukey's post hoc test), suggesting CCI leads to an "all or none" loss of GABAergic cells in this region. GABA cell loss was only observed ipsilateral to the injury and was not observed in the contralateral hemisphere for any treatment group.

To further visualize the extent of interneuron loss following CCI, we next evaluated interneuron density as a function of distance from the injury epicenter for each hippocampal sub-region. For this analysis, we analyzed GFP+ cell density in the ipsilateral hemisphere at the injury site and ± 600 µm in rostral and caudal directions (i.e., transverse sections through 1200 µm of dorsal hippocampus surrounding the injury). To limit bias, sections of CA3 that were 600 µm caudal to the injury were excluded from analysis, because CA3 was no longer orientated in the coronal plane at this distance. In dentate gyrus, interneuron density was significantly reduced throughout the entire dorsal hippocampus (Fig. 2E). However, in CA3 and CA1, the most robust reduction in GFP+ cell density was found within 600 µm rostral to the injury epicenter and GFP+ cell density was not significantly different between injured and uninjured control animals 600 µm caudal to the injury site (Fig. 2F,G). Thus, graded CCI injury produces focal and sub-region specific changes in inhibitory interneuron density in hippocampus.

Hippocampal interneurons show distinct laminar position preferences according to cell type (Freund and Buzsáki, 1996; Klausberger and Somogyi, 2008; Pelkey et al., 2017). Therefore, we next assessed the laminar distribution of GAD67-GFP interneurons 30 days after CCI injury (Fig. 3; **Table S1**), focusing on cells in dentate gyrus or CA1 subfields where interneuron diversity has been well characterized and laminar location anatomically defines specific interneuron subtypes. In dentate gyrus, we found a significant loss of GFP+ cell bodies positioned in the hilus ($F_{(3,17)}$ = 29.03, P = 6.49E-07, n = 5–6 mice per group, one-way ANOVA) and granule cell layer ($F_{(3,17)}$ = 25.00, P = 1.83E-06), but GFP+ cell density was not changed in the molecular layer ($F_{(3,17)}$ = 0.75, P = .54) (Fig. 3A). Loss of GFP+ cells was more extensive following 1.0 mm as compared to 0.5 mm impact depths in this region (**Table S1**), consistent with our finding of graded interneuron loss to increasing injury severity. In CA1, we found a reduction in GFP+ cell bodies positioned in all four cell layers: stratum oriens ($F_{(3,16)}$ = 5.96, P = 6.30E-03, n = 5 mice per group, one-way ANOVA), stratum pyramidale ($F_{(3,16)}$ = 66.91, P = 2.85E-09), stratum radiatum ($F_{(3,16)}$ = 21.61, P = 7.15E-06) and stratum lacunosum-moleculare ($F_{(3,16)}$ = 16.69, P = 3.50E-05) (Fig. 3B). Loss of GFP+ cells was most extensive in the pyramidal cell layer, where both 0.5 mm and 1.0 mm impact depths led to ~50% reduction in GFP+ interneurons (**Table S1**). In dentate gyrus, there was a significant shift in interneuron distribution following CCI, with a larger relative proportion of interneurons found in the molecular layer due to selective survival of

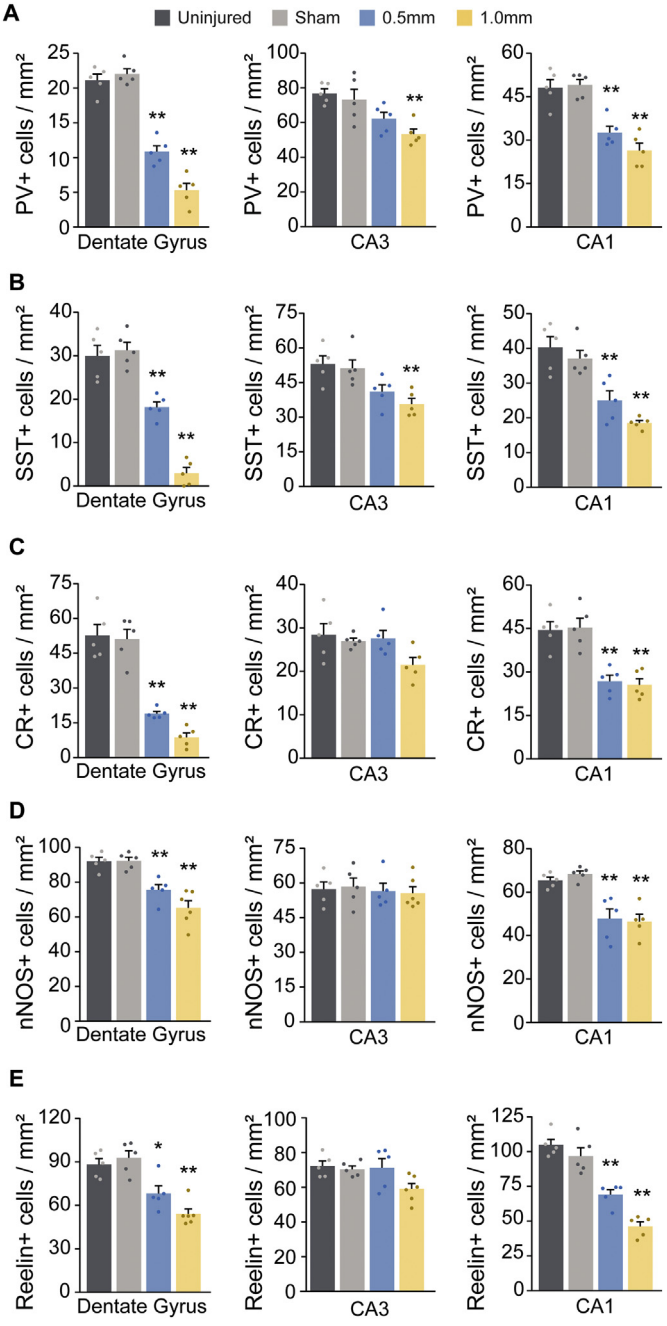

Fig. 5. Selective loss of molecularly-distinct interneuron cohorts following CCI injury. A–E. Quantification of cell density for PV, SST, CR, nNOS and Reelin ipsilateral to the injury in dentate gyrus, CA3 and CA1. Error bars, s.e.m.; *$p < .05$, **$p < .01$.

interneurons in this region ($X^2 = 70.44$, d.f. = 6; $P < .001$; $n = 5$–6 mice per group; Chi-square) (Fig. 3C). A shift in laminar distribution of CA1 interneurons was also detected following CCI ($X^2 = 17.26$, d.f. = 9; $P = .045$; $n = 5$ mice per group; Chi-square).

3.3. Selective loss of molecularly-distinct classes of interneurons after CCI

The constitutive expression of GFP in cells of the GAD67-GFP transgenic mice allows for a systematic investigation of interneurons following neurotrauma. However, interneurons have classically been distinguished based on their unique neurochemical signatures (Freund and Buzsáki, 1996; Pelkey et al., 2017). To delineate the effect of CCI injury on neurochemically-distinct subtypes of interneurons, we performed a series of immunostaining studies 30d after 0.5 mm or 1.0 mm CCI injury using well established markers for hippocampal interneurons (Fig. 4). In dentate gyrus and CA1, we found significant reductions in all cohorts examined (Fig. 5**; Tables S2–6**). Interneuron loss was generally more extensive following 1.0 mm as compared to 0.5 mm impact depths in dentate gyrus, but this was not apparent in CA1. It is important to note that we likely overestimated the loss of CR-containing GABAergic interneurons in dentate gyrus, because large numbers of CR-containing mossy cells are found within the hilus, which are glutamatergic interneurons and especially susceptible to brain injury (Toth et al., 1997). In CA3, we found a significant reduction in the density of neurons expressing PV or SST after 1.0 mm impact, while the density of CR-, nNOS- and reelin–expressing neurons were not changed (Fig. 5C–E**; Tables S2–6**).

Finally, we examined the laminar distribution of each neurochemical marker, focusing on cells within the dentate gyrus and CA1 where interneuron loss is most extensive. In dentate gyrus, there was a significant shift in distribution of markers for PV, nNOS and Reelin following CCI (Fig. 6**, Tables S2–6**). For each cell type, the relative proportion of hilar neurons was reduced and molecular-layer neurons increased (PV: $X^2 = 13.3$, d.f. = 6; $P = .04$; nNOS: $X^2 = 40.4$, d.f. = 6; $P < .001$; Reelin: $X^2 = 52.0$, d.f. = 6; $P < .001$; $n = 5$–6 mice per group; Chi-square), consistent with our findings for GAD67-GFP+ neurons. In CA1, there was also a change in the laminar distribution of PV- and Reelin-expressing cells due to disproportionate reduction of these cell types in the pyramidal cell layer after CCI (PV: $X^2 = 13.3$, d.f. = 6; $P = .04$; Reelin: $X^2 = 22.4$, d.f. = 9; $P = .008$; n = 5 mice per group; Chi-square). Thus, there are graded, regional and cell-type specific changes in the density of hippocampal interneurons following contusive brain injury.

4. Discussion

Neuron loss is a major feature of TBI in both rodents and human (Baldwin et al., 1997; Anderson et al., 2005; Swartz et al., 2006; Hall et al., 2005a,b, 2008; Buriticá et al., 2009), but the loss of interneurons following contusive injury has not been systematically evaluated. Our results provide the first comprehensive analysis of hippocampal interneurons following graded CCI injury. We found a dramatic reduction in interneuron density that was dependent on impact depth, hippocampal sub-region and laminar position. In agreement with these findings, analysis of neurochemically distinct cohorts of interneurons revealed cell type-specific vulnerability to head injury. Interneurons located in the principal cell and polymorph layers (e.g., PV and SST) were generally more vulnerable to injury than cell types occupying the molecular layer (e.g., nNOS and Reelin). This was observed most clearly in dentate gyrus. Overall, our results demonstrate a reorganization of interneuron diversity following contusion injury that may substantially alter information processing within hippocampal circuits.

Each sub-region of hippocampus displayed a different histological response to CCI injury. In dentate gyrus, interneuron loss correlated quantitatively with contusion depth, consistent with our prior work demonstrating mossy fiber sprouting and seizures are more robust with increasing impact depths (Hunt et al., 2009, 2010, 2012). While mossy fiber sprouting does not correlate with seizure frequency (Buckmaster and Dudek, 1997), loss of interneurons does (Buckmaster et al., 2017). This may explain the relatively high incidence of seizures following CCI injury as compared to other neurotrauma models (Hunt et al., 2009, 2010; Nichols et al., 2014; Semple et al., 2017). Although previous studies have reported substantial neuron dystrophy and loss in the CA3 sub-region (Baldwin et al., 1997; Anderson et al., 2005), we found interneurons in CA3 were relatively well preserved compared to other hippocampal regions. These differences might be explained by the histological analyses employed (e.g., Fluoro-Jade and NeuroSilver staining versus markers for interneurons). Indeed, most prior studies evaluating regional hippocampal damage have focused on principal

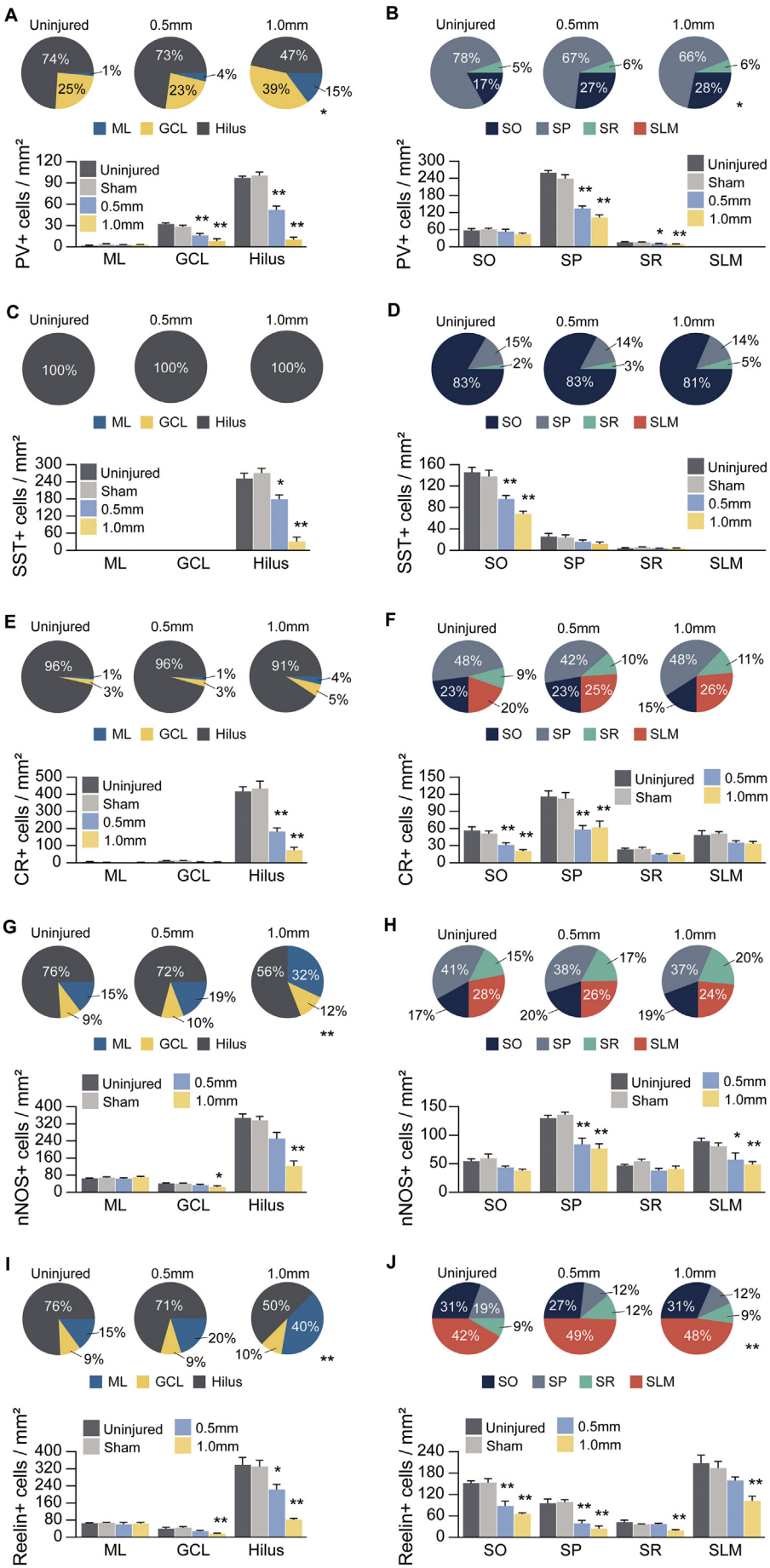

Fig. 6. CCI produces cell type-specific changes in interneuron distribution. A,C,E,G,I. Quantification of neurons expressing PV, SST, CR, nNOS and Reelin in dentate gyrus ipsilateral to the injury. Pie charts show proportion of neurons found in each cell layer, and bar plots show cell densities in each layer. **B,D,F,H,J.** Quantification of neurons expressing PV, SST, CR, nNOS and Reelin in CA1 ipsilateral to the injury. Pie charts show relative proportion of neurons found in each cell layer, and bar plots show cell densities in each layer. ML, molecular layer; GCL, granule cell layer; SO, stratum oriens; SP, stratum pyramidale; SR, stratum radiatum; SLM, stratum lacunosum-moleculare. Error bars, s.e.m.; $*p < .05$, $**p < .01$.

neurons, and Fluoro-Jade B staining appears most robust in principal neuron populations in the first week after CCI (Anderson et al., 2005; Hall et al., 2008). Another possibility is that varying external injury parameters between studies might produce differences in regional cell damage after CCI. In our studies, we positioned the impactor tip parallel to midline, which in our hands leads to a substantial lesion to granule cells and CA1 pyramids, but not CA3 (Hall et al., 2008; Hunt et al., 2009, 2012). Prior studies reporting extensive CA3 damage have angled the head (or impactor) to deliver an injury perpendicular to the surface of the cortex (Anderson et al., 2005; Saatman et al., 2006). Computer models show shifting the angle of impact applies more tissue strain to the CA3 region (Mao et al., 2010; Mao and Yang, 2011). However, further investigation is needed to clarify the role of tissue level biomechanics on regional interneuron loss.

Functionally, CCI injury leads to a reduction in synaptic inhibition in hippocampus (Hunt et al., 2010; Almeida-Suhett et al., 2014, 2015; Butler et al., 2016). This is likely due to loss of interneurons as well as changes in the expression of $GABA_A$ receptor subunits (Raible et al., 2015) and subtype-specific modifications of inhibitory circuits. We previously reported a shift from somatic to dendritic inhibition in dentate granule cells following CCI injury (Hunt et al., 2011). Our current data reveal a proportional preservation of molecular layer interneurons, which primarily target dendrites. Together, these findings suggest there may be a domain-specific shift from feedback to feedforward GABAergic inhibition after TBI, at least in dentate gyrus circuits. The computational consequences of such a shift are unknown, but at a circuit level, one might expect inhibitory drive is more capable of shunting excitatory input than synchronizing principal cell populations in the injured dentate gyrus. Alternatively, dendrite-projecting GABA neurons are involved in timing rhythmic cortical cell discharges (Szabadics et al., 2001) and can drive ictogenesis (Wendling et al., 2002). Thus, network level studies are ultimately necessary to determine how long-term changes in interneuron diversity affect the activity dynamics of principal neurons in vivo.

Successful therapeutic approaches for TBI will ultimately depend on cellular mechanisms of the initial insult and cell type-specific modifications of injured neural circuitry (Hunt et al., 2013). As such, it is critically important to understand which cell populations are sensitive to neurotrauma and how the cellular environment changes. Our results provide an important step in understanding the response of hippocampal interneurons to contusive brain injury.

Acknowledgements

This work was supported by funding from the National Institutes of Health grants NINDS R00–NS085046, R01–NS096012 and T32–NS045540 and T32–NS082174. We thank Daniel Vogt and John Rubenstein for kindly sharing GAD67-GFP mice.

Author contributions

R.F.H. and J.C.F. designed research; J.C.F. and Y.J.K. performed experiments; R.F.H., and J.C.F. analyzed data; R.F.H. and J.C.F. wrote the manuscript; J.C.F. and Y.J.K. edited the manuscript.

Appendix A. Supplementary data

Supplementary data to this article can be found online at https://doi.org/10.1016/j.nbd.2018.07.022.

References

Almeida-Suhett, C.P., Prager, E.M., Pidoplichko, V., Figueiredo, T.H., Marini, A.M., Li, Z., Eiden, L.E., Braga, M.F., 2014. Reduced GABAergic inhibition in the basolateral amygdala and the development of anxiety-like behaviors after mild traumatic brain injury. PLoS One 9, e102627.

Almeida-Suhett, C.P., Prager, E.M., Pidoplichko, V., Figueiredo, T.H., Marini, A.M., Li, Z., Eiden, L.E., Braga, M.F., 2015. GABAergic interneuronal loss and reduced inhibitory synaptic transmission in the hippocampal CA1 region after mild traumatic brain injury. Exp. Neurol. 273, 11–23.

Anderson, K.J., Miller, K.M., Fugaccia, I., Scheff, S.W., 2005. Regional distribution of fluoro-jade B staining in the hippocampus following traumatic brain injury. Exp. Neurol. 193, 125–130.

Baldwin, S.A., Gibson, T., Callihan, C.T., Sullivan, P.G., Palmer, E., Scheff, S.W., 1997. Neuronal cell loss in the CA3 subfield of the hippocampus following cortical contusion utilizing the optical disector method for cell counting. J. Neurotrauma 14, 385–398.

Buckmaster, P.S., Dudek, F.E., 1997. Neuron loss, granule cell axon reorganization, and functional changes in the dentate gyrus of epileptic kainate-treated rats. J. Comp. Neurol. 385, 385–404.

Buckmaster, P.S., Abrams, E., Wen, X., 2017. Seizure frequency correlates with loss of dentate gyrus GABAergic neurons in a mouse model of temporal lobe epilepsy. J. Comp. Neurol. 525, 2592–2610.

Buriticá, E., Villamil, L., Guzmán, F., Escobar, M.I., García-Cairasco, N., Pimienta, H.J., 2009. Changes in calcium-binding protein expression in human cortical contusion tissue. J. Neurotrauma 26, 2145–2155.

Butler, C.R., Boychuk, J.A., Smith, B.N., 2016. Differential effects of rapamycin treatment on tonic and phasic GABAergic inhibition in dentate granule cells after focal brain injury in mice. Exp. Neurol. 280, 30–40.

Cantu, D., Walker, K., Andresen, L., Taylor-Weiner, A., Hampton, D., Tesco, G., Dulla, C.G., 2015. Traumatic brain injury increases cortical glutamate network activity by compromising GABAergic control. Cereb. Cortex 25, 2306–2320.

Centers for Disease Control and Prevention, 2015. Report to Congress on Traumatic Brain Injury in the United States: Epidemiology and Rehabilitation. National Center for Injury Prevention and Control; Division of Unintentional Injury Prevention, Atlanta, GA.

de Lanerolle, N.C., Kim, J.H., Robbins, R.J., Spencer, D.D., 1989. Hippocampal interneuron loss and plasticity in human temporal lobe epilepsy. Brain Res. 495, 387–395.

Dinday, M.T., Girskis, K.M., Lee, S., Baraban, S.C., Hunt, R.F., 2017. PAFA1B1 haploinsufficiency disrupts GABA neurons and synaptic E/I balance in the dentate gyrus. Sci. Rep. 7, 8269.

Faul, M., Xu, L., Wald, M.M., Coronado, V.G., 2010. Traumatic Brain Injury in the United States: Emergency Department Visits, Hospitalizations, and Deaths. National Center for Injury Prevention and Control, Centers for Disease Control and Prevention.

Frankowski, J.C., Hunt, R.F., 2018. Modeling traumatic brain injury using controlled cortical impact injury. In: KOPF Carrier. #93.

Freund, T.F., Buzsáki, G., 1996. Interneurons of the hippocampus. Hippocampus 6 (4), 347–470.

Frey, L.C., 2003. Epidemiology of posttraumatic epilepsy: a critical review. Epilepsia 44, S11–S17.

Gupta, A., Elgammal, F.S., Proddutur, A., Shah, S., Santhakumar, V., 2012. Decrease in tonic inhibition contributes to increase in dentate semilunar granule cell excitability after brain injury. J. Neurosci. 32, 2523–2537.

Hall, E.D., Gibson, T.R., Pavel, K.M., 2005a. Lack of a gender difference in post-traumatic neurodegeneration in the mouse contolled cortical impact injury model. J. Neurotrauma 22, 669–679.

Hall, E.D., Sullivan, P.G., Gibson, T.R., Pavel, K.M., Thompson, B.M., Scheff, S.W., 2005b. Spatial and temporal characteristics of neurodegeneration after controlled cortical impact in mice: more than a focal brain injury. J. Neurotrauma 22, 252–265.

Hall, E.D., Bryant, Y.D., Cho, W., Sullivan, P.G., 2008. Evolution of post-traumatic neurodegeneration after controlled cortical impact traumatic brain injury in mice and rats as assessed by the de Olmos silver and fluorojade staining methods. J. Neurotrauma 25, 235–247.

Herman, S.T., 2002. Epilepsy after brain insult: targeting epileptogenesis. Neurology 59, S21–S26.

Hunt, R.F., Scheff, S.W., Smith, B.N., 2009. Posttraumatic epilepsy after controlled cortical impact injury in mice. Exp. Neurol. 215, 243–252.

Hunt, R.F., Scheff, S.W., Smith, B.N., 2010. Regionally localized recurrent excitation in the dentate gyrus of a cortical contusion model of posttraumatic epilepsy. J. Neurophysiol. 103, 1490–1500.

Hunt, R.F., Scheff, S.W., Smith, B.N., 2011. Synaptic reorganization of inhibitory hilar interneuron circuitry after traumatic brain injury in mice. J. Neurosci. 31, 6880–6890.

Hunt, R.F., Haselhorst, L.A., Schoch, K.M., Bach, E.C., Rios-Pilier, J., Scheff, S.W., Saatman, K.E., Smith, B.N., 2012. Posttraumatic mossy fiber sprouting is related to the degree of cortical damage in three mouse strains. Epilepsy Res. 99, 167–170.

Hunt, R.F., Boychuk, J.A., Smith, B.N., 2013. Neural circuit mechanisms of post-traumatic epilepsy. Front. Cell. Neurosci. 7, 89.

Huusko, N., Römer, C., Ndode-Ekane, X.E., Lukasiuk, K., Pitkänen, A., 2015. Loss of hippocampal interneuron and epileptogenesis: a comparison of two animal models of acquired epilepsy. Brain Struct. Funct. 220, 153–191.

Klausberger, T., Somogyi, P., 2008. Neuronal diversity and temporal dynamics: the unity of hippocampal circuit operations. Science 321, 53–57.

Li, H., Prince, D.A., 2002. Synaptic activity in chronically injured, epileptogenic sensory-motor neocortex. J. Neurophysiol. 88, 2–12.

Liepert, J., Storch, P., Fritsch, A., Weiller, C., 2000. Motor cortex disinhibition in acute stroke. Clin. Neurophysiol. 111, 671–676.

Lowenstein, D.H., Thomas, M.J., Smith, D.H., McIntosh, T.K., 1992. Selective vulnerability of dentate hilar neurons following traumatic brain injury: a potential mechanicstic ink between head trauma and disorders of the hippocampus. J. Neurosci. 12, 4846–4853.

Mao, H., Yang, K.H., 2011. Investigation of brain contusion mechanism and threshold by

combining finite element analysis with in vivo histology data. Int. J. Numeri. Method Biomed. Eng. 24, 357–366.
Mao, H., Yang, K.H., King, A.I., Yang, K., 2010. Computational neurotrauma - design, simulation, and analysis of controlled cortical impact model. Biomech. Model. Mechanobiol. 9, 763–772.
Nichols, J., Perez, R., Wu, C., Adelson, P.D., Anderson, T., 2014. Traumatic brain injury induces rapid enhancement of cortical excitability in juvenile rats. CNS Neurosci. Ther. 2, 193–203.
Nichols, J., Bjorklund, G.R., Newbern, J., Anderson, T., 2018. Parvalbumin fast-spiking interneurons are selectively altered by pediatric traumatic brain injury. J. Physiol. 596, 1277–1293.
Pavlov, I., Huusko, N., Drexel, M., Kirchmair, E., Sperk, G., Pitkänen, A., Walker, M.C., 2011. Progressive loss of phasic, but not tonic, GABAA receptor-mediated inhibition in dentate granule cells in a model of post-traumatic epilepsy in rats. Neuroscience 194, 208–219.
Pelkey, K.A., Chittajallu, R., Craig, M.T., Tricoire, L., Wester, J.C., McBain, C.J., 2017. Hippocampal GABAergic inhibitory interneurons. Physiol. Rev. 97, 1619–1747.
Pleasant, J.M., Carlson, S.W., Mao, H., Scheff, S.W., Yang, K.H., Saatman, K.E., 2011. Rate of neurodegeneration in the mouse controlled cortical impact model is influenced by impactor tip shape: implications for mechanistic and therapeutic studies. J. Neurotrauma 28, 2245–2262.
Raible, D.J., Frey, L.C., Del Angel, Y.C., Carlsen, J., Hund, D., Russek, S.J., Smith, B., Brooks-Kayal, A.R., 2015. JAK/STAT pathway regulation of GABAA receptor expression after differing severities of experimental TBI. Exp. Neurol. 271, 445–456.
Rao, V., Lyketsos, C., 2000. Neuropsychiatric sequalae of traumatic brain injury. Psychosomatics 41, 95–103.
Saatman, K.E., Feeko, K.J., Pape, R.L., Raghupathi, R., 2006. Differential behavioral and histopathological responses to graded cortical impact injury in mice. J. Neurotrauma 23, 1241–1253.
Santhakumar, V., Bender, R., Frotscher, M., Ross, S.T., Hollrigel, G.S., Toth, Z., Soltesz, I., 2000. Granule cell hyperexcitability in the early post-traumatic rat dentate gyrus: the 'irritable mossy cell' hypothesis. J. Physiol. 254, 117–134.
Satoh, J., Tabira, T., Sano, M., Nakayama, H., Tateishi, J., 1991. Parvalbumin-immunoreactive neurons in the human central nervous system are decreased in Alzheimer's disease. Acta Neuropathol. 81, 338–395.
Scholten, A.C., Haagsma, J.A., Andriessen, T.M., Vos, P.E., Steyerberg, E.W., Van Beeck, E.F., Polinder, S., 2015. Health-related quality of life after mild, moderate and severe traumatic brain injury: patterns and predictors of suboptimal functioning during the first year after injury. Injury 46, 616–624.
Semple, B.D., O'Brien, T.J., Gimlin, K., Wright, D.K., Kim, S.E., Casillas-Espinosa, P.M., Webster, K.M., Petrou, S., Noble-Haeussiein, L.J., 2017. Interleukin-1 receptor in seizure susceptibility after traumatic injury to the pediatric brain. J. Neurosci. 37, 7864–7877.
Swartz, B.E., Houser, C.R., Tomiyasu, U., Walsh, G.O., DeSalles, A., Rich, J.R., Delgado-Escueta, A., 2006. Hippocampal cell loss in posttraumatic human epilepsy. Epilepsia 47, 1373–1382.
Szabadics, J., Lorincz, A., Tamás, G., 2001. Beta and gamma frequency synchronization by dendritic GABAergic synapses and gap junctions in a network of cortical interneurons. J. Neurosci. 21, 5824–5831.
Tamamaki, N., Yanagawa, Y., Tomioka, R., Miyazaki, J.I., Obata, K., Kaneko, T., 2003. Green fluorescent protein expression and colocalization with calretinin, parvalbumin, and somatostatin in the GAD67-GFP knock-in mouse. J. Comp. Neurol. 467, 60–79.
Toth, Z., Hollrigel, G.S., Gorcs, T., Soltesz, I., 1997. Instantaneous perturbation of dentate interneuronal networks by a pressure wave-transient delivered to the neocortex. J. Neurosci. 17, 8106–8117.
Wendling, F., Bartolomei, F., Bellanger, J.J., Chauvel, P., 2002. Epileptic fast activity can be explained by a model of impaired GABAergic dendritic inhibition. Eur. J. Neurosci. 15, 1499–1508.